

## Argon nucleation: Bringing together theory, simulations, and experiment

V. I. Kalikmanov,<sup>1,a)</sup> J. Wölk,<sup>2</sup> and T. Kraska<sup>2</sup><sup>1</sup>*Twister Supersonic Gas Solutions, Einsteinlaan 10, 2289 CC, Rijswijk, The Netherlands*<sup>2</sup>*Institute for Physical Chemistry, University of Cologne, D-50939 Cologne, Germany*

(Received 28 November 2007; accepted 5 February 2008; published online 25 March 2008)

We present an overview of the current status of experimental, theoretical, molecular dynamics (MD), and density functional theory (DFT) studies of argon vapor-to-liquid nucleation. Since the experimental temperature-supersaturation domain does not overlap with the corresponding MD and DFT domains, separate comparisons have been made: theory versus experiment and theory versus MD and DFT. Three general theoretical models are discussed: Classical nucleation theory (CNT), mean-field kinetic nucleation theory (MKNT), and extended modified liquid drop model-dynamical nucleation theory (EMLD-DNT). The comparisons are carried out for the area below the MKNT pseudospinodal line. The agreement for the nucleation rate between the nonclassical models and the MD simulations is very good—within 1–2 orders of magnitude—while the CNT deviates from simulations by about 3–5 orders of magnitude. Perfect agreement is demonstrated between DFT results and predictions of MKNT (within one order of magnitude), whereas CNT and EMLD-DNT show approximately the same deviation of about 3–5 orders of magnitude. At the same time the agreement between all theoretical models and experiment remains poor—4–8 orders of magnitude for MKNT, 12–14 orders for EMLD-DNT, and up to 26 orders for CNT. We discuss possible reasons for this discrepancy and the ways to carry out experiment and simulations within the common temperature-supersaturation domain in order to produce a unified picture of argon nucleation. © 2008 American Institute of Physics. [DOI: 10.1063/1.2888995]

### I. INTRODUCTION

Argon plays an exceptional role in various areas of soft condensed matter physics. It belongs to the class of simple fluids whose behavior on molecular level can be adequately described by the Lennard-Jones (LJ) potential. Equilibrium properties of argon have been extensively studied experimentally,<sup>1</sup> theoretically,<sup>2,3</sup> in computer simulations—Monte Carlo (MC) and molecular dynamics<sup>4,5</sup> (MD) and by means of the density functional theory (DFT).<sup>6,7</sup>

Argon represents an important system also for nonequilibrium studies. In this context the phenomenon of nucleation is of special significance. Theoretical description of nucleation is a complicated matter. The current situation with nucleation theories is such that no theoretical model can successfully quantitatively describe nucleation of all substances under various external conditions. In this situation argon can play a role of the test substance for which experimental, theoretical, and simulation efforts can be combined in order to obtain a better insight into the nucleation phenomenon and abilities of various approaches to adequately describe it.

Despite the exclusive importance of argon it has only recently become possible to carry out argon nucleation experiments—thanks to the construction of the cryogenic nucleation pulse chamber in the group of Strey in the University of Cologne,<sup>8</sup> and its further development.<sup>9</sup> This chamber uses a deep adiabatic expansion of the argon-helium mixture which causes argon nucleation at temperatures below the triple point.

During recent years, a spectrum of theoretical models of nucleation has been significantly broadened. It has been widely recognized that the properties of small clusters play a crucial role in the description of nucleation behavior. For small clusters the concepts of macroscopic surface tension and surface area lose their meaning and therefore the use of the capillarity approximation, which is the main assumption of the classical nucleation theory (CNT) of Becker, Döring, and Zeldovich,<sup>10</sup> becomes fundamentally in error. Starting with the work of Lee *et al.*,<sup>11</sup> various approaches have been proposed to calculate the free energy of clusters of arbitrary size. These include the DFT of nucleation developed by Oxtoby and co-workers,<sup>12,13</sup> the introduction of an  $i, v$  cluster by Reiss and co-workers,<sup>14</sup> and the dynamic nucleation theory (DNT) of Schenter *et al.*<sup>15,16</sup> These developments require the knowledge of an intermolecular potential which for most of the substances is not available. For this reason the CNT, despite its shortcomings, still remains the most widely used theoretical model.

A compromise between the microscopic and the phenomenological approaches was proposed by Dillmann and Meier<sup>17</sup> and later developed by various authors.<sup>18</sup> In these, semiphenomenological, nucleation models the free energy of cluster formation is derived from the statistical thermodynamics of clusters using the seminal Fisher droplet model of condensation.<sup>19</sup> The effect of curvature on the surface free energy of the cluster is taken into account by expanding the surface tension of a cluster in powers of its curvature. The first order term of this expansion is known as the Tolman correction.<sup>2</sup> However, recent DFT calculations by Koga *et al.*<sup>20</sup> revealed that the Tolman correction becomes

<sup>a)</sup>Electronic mail: vitaly.kalikmanov@twisterbv.com.

valid for clusters, containing  $>10^5$  particles, indicating that it is of minor importance for typical conditions of nucleation experiments where critical clusters contain few tens or hundreds of molecules.

An alternative way to calculate the surface free energy of an arbitrary cluster has been recently proposed by one of us within the framework of the mean-field kinetic nucleation theory (MKNT).<sup>21</sup> This theory is by construction nonperturbative in a cluster curvature and as such is valid for all clusters down to monomers. Another modification of the classical approach—the extended modified liquid drop model-dynamical nucleation theory (EMLD-DNT)—has been recently put forward by Reguera and Reiss.<sup>22</sup> It represents the combination of the EMLD of Reguera *et al.*<sup>23</sup> with the DNT of Schenter *et al.*<sup>15</sup> The model proposes a definition of the cluster which properly takes into account fluctuations. The advantage of EMLD-DNT is that it uses the same set of macroscopic parameters as the CNT. In the present paper for the theoretical description of argon nucleation we use three models—CNT, MKNT, and EMLD-DNT.

An important source of information on nucleation in simple fluids is MD and MC simulations. In this paper we refer to the recent MD simulations of argon nucleation in the microcanonical (*NVE*) ensemble<sup>24</sup> and the isokinetic (*NVT*) ensemble.<sup>25</sup> We also discuss the mean-field DFT calculations of nucleation in LJ fluids by Zeng and Oxtoby.<sup>13</sup> Those were carried out for relatively high temperatures  $83 < T < 130$  K which only partly cover the temperature range of the MD simulations mentioned earlier.

## II. TEMPERATURE-SUPERSATURATION DOMAIN: EXPERIMENTS, SIMULATIONS AND DFT

We start the discussion of argon nucleation by identifying the domain of the parameters—temperature  $T$  and supersaturation  $S = p/p_{\text{sat}}(T)$ —for which experiments, simulations, and DFT studies were carried out. Here  $p$  and  $p_{\text{sat}}(T)$  are the actual vapor pressure and the saturation pressure of argon, respectively. This domain is shown in Fig. 1. Open squares in this figure correspond to the experiments of Iland *et al.*<sup>9</sup> performed for the temperature range  $40 \text{ K} < T < 60 \text{ K}$  and supersaturations  $2 < \ln S < 5$ . The resulting onset nucleation rate was estimated in Ref. 9 as  $\log_{10} J_{\text{expt}}/\text{cm}^{-3} \text{ s}^{-1} = 7 \pm 2$ . MD/*NVE* simulations<sup>24</sup> (filled squares) cover a broader temperature range  $30 \text{ K} < T < 85 \text{ K}$ . However, to get good statistics of rare nucleation events, simulations were performed for extremely high supersaturations (far beyond the experimental values of Ref. 9) resulting in the nucleation rates in the range of  $\log_{10} J_{\text{MD}}/\text{cm}^{-3} \text{ s}^{-1} = 25\text{--}29$ . The same remark refers to MD/*NVT* simulations<sup>25</sup> (filled rhombs) performed for the temperature range  $45 \text{ K} < T < 70 \text{ K}$  with the nucleation rates in the range of  $\log_{10} J_{\text{MD}}/\text{cm}^{-3} \text{ s}^{-1} = 23\text{--}25$ . Closed circles in Fig. 1 correspond to the DFT calculations of Zeng and Oxtoby<sup>13</sup> carried out for high temperatures  $83 \text{ K} < T < 130 \text{ K}$  and low  $S$ ; the value of  $S$  in Ref. 13 was chosen such that the CNT nucleation rate is  $J_{\text{CNT}} = 1 \text{ cm}^{-3} \text{ s}^{-1}$ .

Discussing the values of  $S$  one should keep in mind that they are limited from above by the spinodal which denotes

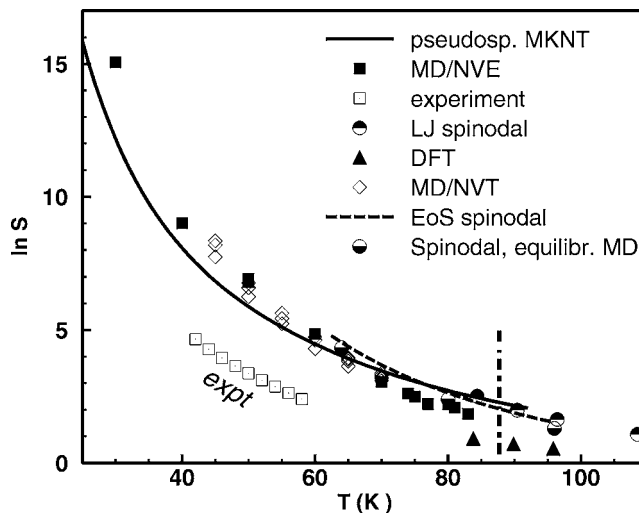


FIG. 1.  $T$ - $S$  domain of: experiment of Iland *et al.* (Ref. 9) (open squares), MD/*NVE* simulations (Ref. 24) (filled squares), MD/*NVT* simulations (Ref. 25) (open rhombs), and DFT simulations of Zeng and Oxtoby (Ref. 13) (filled triangles). Also shown is the MKNT pseudospinodal given by Eq. (7) (solid line), the LJ vapor spinodal data from MD simulations of Linhart *et al.* (Ref. 28) (upper half-filled circles), the spinodal data obtained from equilibrium MD simulations of Imre *et al.* (Ref. 31) (lower half-filled circles), and the spinodal line from the LJ EoS of Kolafa and Nezbeda (Ref. 27) (dashed line). The vertical dashed-dotted line denotes the upper temperature limit for the applicability of the MKNT.

the limit of thermodynamic stability of the fluid. One can estimate the spinodal from a suitable equation of state (EoS).<sup>26</sup> The spinodal calculated from the LJ EoS of Kolafa and Nezbeda<sup>27</sup> is added in Fig. 1 (dashed line). Extrapolations below the triple point are limited because EoS are usually fitted to experimental data in the stable region only. Recently, Linhart *et al.*<sup>28</sup> performed MD simulations of the supersaturated vapor of a LJ fluid and obtained the spinodal pressure for the temperature range  $0.7 \leq k_B T / \epsilon_{\text{LJ}} \leq 1.2$ , where  $\epsilon_{\text{LJ}}$  is the LJ energy parameter. This temperature range corresponds to  $84 \text{ K} < T < 143 \text{ K}$  for argon. They estimated the spinodal by the appearance of an instantaneous phase separation in the supersaturated vapor increasing the argon density in a series of simulations. Simulations were performed for a very large cutoff radius  $10\sigma_{\text{LJ}}$ , where  $\sigma_{\text{LJ}}$  is the LJ size parameter and nonshifted LJ potential. A large cutoff radius makes it feasible to apply the simulation results to real argon. It has been shown that the usually used cutoff radii of  $5\sigma_{\text{LJ}}$  and  $6.5\sigma_{\text{LJ}}$  are sufficient,<sup>29</sup> while  $2.5\sigma_{\text{LJ}}$  gives significant deviation in the thermophysical properties.<sup>30</sup> The values of the spinodal supersaturation resulting from Ref. 28 are shown by upper half-filled circles. Unfortunately, simulations of Ref. 28 cover only partially the temperature domain of MD simulations of Refs. 24 and 25 and DFT of Ref. 13. In a recent work<sup>31</sup> the argon spinodal is estimated using a new MD-based approach from the extremes of the tangential component of the pressure tensor obtained from the simulations of the vapor-liquid interface. This is a rather simple approach based on single equilibrium simulation without any constraints and also applicable below the triple point. The corresponding values are shown in Fig. 1 by lower half-filled circles.

Within the spinodal region the fluid becomes unstable

giving rise to the phenomenon of spinodal decomposition. The latter is characterized by the zero barrier of critical cluster formation. However, in practice this limit is hard to achieve: gradual quenching of the supersaturated vapor results in the barrier becoming equal to the characteristic value of natural thermal fluctuations of the free energy, which in a fluid is of the order of  $k_B T$ , where  $k_B$  is the Boltzmann constant. With this in mind, we show in Fig. 1 the pseudospinodal,  $\ln S_{\text{psp}}^{\text{MKNT}}$  (solid line), resulting from the MKNT,<sup>21,32</sup> which corresponds to the free energy barrier of the critical cluster formation  $\Delta G^* \approx k_B T$ . At  $S = S_{\text{psp}}^{\text{MKNT}}$ , the phase separation proceeds not via nucleation but via the mechanism of spinodal nucleation<sup>33</sup> which differs both from nucleation and spinodal decomposition. Therefore, the actual, experimentally realizable, upper limit of  $S$  for nucleation is the pseudospinodal and not the spinodal. As one can see from Fig. 1, the LJ spinodal obtained from an EoS (Refs. 26 and 27) and MD simulations<sup>28,31</sup> are close to the MKNT pseudospinodal within its range of validity (discussed in Sec. III B), which for argon is  $T < 92$  K (vertical dashed-dotted line). Equilibrium thermodynamic properties of argon are those of Ref. 9 (for clarity they are presented in the Appendix).

After a brief description of the theoretical models used in the present paper, we compare in Sec. IV the results of theories, experiment, simulations, and DFT calculations within the  $T$ – $S$  domain bounded from above by the pseudospinodal  $\ln S_{\text{psp}}^{\text{MKNT}}(T)$  and for the temperatures  $T < 92$  K corresponding to the range of validity of MKNT [given by Eq. (8) in Sec. III B].

### III. THEORETICAL MODELS

#### A. CNT

In CNT the Gibbs free energy of the  $n$ -cluster formation is written using the capillarity approximation as<sup>34</sup>

$$\beta \Delta G_{\text{CNT}}(n) = -n \ln S + \theta_{\infty} n^{2/3}, \quad \beta = 1/k_B T. \quad (1)$$

Here  $\theta_{\infty}(T) = \beta \gamma_{\infty} s_1$  is the reduced macroscopic surface tension,  $\gamma_{\infty}$  is the dimensional macroscopic surface tension,  $s_1 = 4\pi(r^l)^2$ ,  $r^l = (3/4\pi\rho^l)^{1/3}$  is the mean intermolecular distance in the liquid phase, and  $\rho^l$  is the liquid number density at the temperature  $T$ . The CNT result for the nucleation rate is<sup>34</sup>

$$J_{\text{CNT}} = K_{\text{CNT}} \exp\left(-\frac{\Delta G_{\text{CNT}}^*}{k_B T}\right),$$

where the free energy barrier of the critical cluster formation and the kinetic prefactor read

$$\Delta G_{\text{CNT}}^* \equiv \Delta G_{\text{CNT}}(n_c) = \frac{16\pi}{3} \frac{\gamma_{\infty}^3}{(\rho^l k_B T \ln S)^2},$$

$$K_{\text{CNT}} = \frac{(\rho^v)^2}{\rho^l} \sqrt{\frac{2\gamma_{\infty}}{\pi m_1}}.$$

Here  $n_c$  is the number of molecules in the critical cluster,  $m_1$  is a mass of a molecule,  $\rho^v$  is the supersaturated vapor number density.

#### B. Main features of the MKNT

MKNT (Ref. 21) is a semiphenomenological model, which is nonperturbative in the cluster size, and as such is valid for arbitrary clusters. By construction it is an interpolative model between very small clusters treated using statistical mechanical considerations and large clusters described by the phenomenological capillarity approximation. MKNT uses six input material parameters: four phenomenological parameters— $p_{\text{sat}}(T)$ ,  $\rho^l(T)$ ,  $\gamma_{\infty}(T)$ , and the second virial coefficient  $B_2(T)$ —and two microscopic quantities—the characteristic molecular size  $\sigma$  and the depth of intermolecular interactions  $\epsilon$ . Note that the first three phenomenological parameters are the same as in the CNT. Using these quantities one constructs two reduced surface tensions: the bulk reduced surface tension (the same as in the CNT),  $\theta_{\infty}(T)$  and the microscopic reduced surface tension

$$\theta_{\text{micro}}(T) = -\ln\left(-\frac{B_2 p_{\text{sat}}}{k_B T}\right), \quad (2)$$

the latter being the reduced specific free energy per surface molecule in the cluster. As seen from Eq. (2),  $\theta_{\text{micro}}$  reflects the nonideality of the vapor which is described by the second virial coefficient.

A cluster in MKNT is characterized by the number of molecules  $n$  (rather than by its radius). The cluster is considered to consist of the two groups of molecules: the core  $n^{\text{core}}$  and the surface molecules  $n^s$ :  $n = n^{\text{core}} + n^s$ . The physical idea behind this distinction is that the core, if present, should possess the liquidlike structure which can be characterized by the coordination number in the liquid phase  $N_1$ . Both  $n^{\text{core}}$  and  $n^s$  fluctuate around their mean values:  $n^{\text{core}} = \overline{n^{\text{core}}}(n; T) + \delta n^{\text{core}}$ ,  $n^s = \overline{n^s}(n; T) + \delta n^s$ , so that  $\delta n^{\text{core}} + \delta n^s = 0$ . The quantity  $\overline{n^s}(n)$  is determined for all values of  $n$ . For small clusters

$$\overline{n^s}(n) = n, \quad \text{for } n \leq N_1 \quad (3)$$

and  $\overline{n^{\text{core}}} = 0$  showing that clusters with  $n \leq N_1$  do not possess liquidlike properties; they do not have a core and all their molecules belong to the surface.

For  $n \geq N_1 + 1$  an  $n$  cluster has a core containing on average  $\overline{n^{\text{core}}}(n)$  particles and characterized by a radius  $R^{\text{core}}$  and the number density  $\rho^l$ . The surface layer, containing on average  $\overline{n^s}(n)$  particles, is characterized by a thickness  $\lambda r^l$ ,  $\lambda \geq 1$ , and the constant density  $\xi \rho^l$  with  $0 < \xi \leq 1$ . One can view the surface molecules as an “adsorption layer for the core” separating it from the bulk vapor surrounding the cluster (note that  $\lambda = 1$  corresponds to a monolayer of surface particles). We stress that this division is purely schematic and serves the purposes of the model. Thus, for  $n \geq N_1 + 1$ , the actual (unknown) smooth density profile is replaced in MKNT by a two-step function with the middle step corresponding to the surface layer(s) while the CNT approximates a cluster by a sharp single-step profile.

Introducing the dimensionless core radius  $x = R^{\text{core}}/r^l$  we have

$$\overline{n^s}(n) = n - [x(n)]^3, \quad \text{for } n \geq N_1 + 1. \quad (4)$$

It is more convenient to use the pair of temperature dependent material parameters  $\lambda$  and  $\omega \equiv \xi \lambda$  instead of the pair

$(\lambda, \xi)$ . Then  $x(n)$  in Eq. (4) is the real positive root of the cubic equation

$$x^3 = -3\omega x^2 - 3\omega\lambda x + (n - \omega\lambda^2). \quad (5)$$

The parameters,  $\lambda$  and  $\omega$ , of order unity, are found from the relationships<sup>21</sup>

$$\omega = \frac{1}{3} \frac{\theta_\infty}{\theta_{\text{micro}}},$$

$$\lambda = \sqrt{\frac{N_1}{\omega} - \frac{3}{4} - \frac{3}{2}}.$$

By construction  $x(n=N_1+1)=1$ , meaning that when the number of molecules in the cluster exceeds  $N_1$  the core starts to grow, for  $n=N_1+1$  it contains exactly one molecule. Since information about  $N_1$  is not always available, it can be obtained from an approximation in which  $N_1$  is expressed in terms of the molecular packing fraction in the liquid phase

$$\eta = (\pi/6)\rho^l d_{\text{hs}}^3,$$

where  $d_{\text{hs}}(T; \sigma, \epsilon)$  is the effective hard sphere diameter in the theory of liquids. The dependence  $N_1(\eta)$  for  $4 \leq N_1 \leq 8$ , which is a typical range of coordination numbers in the liquid phase, is well approximated by (for the details see Ref. 21)

$$N_1 = 5.5116\eta^2 + 6.1383\eta + 1.275.$$

The quantity  $d_{\text{hs}}(T)$  is given by the Barker–Henderson relation with the Weeks–Chandler–Anderson decomposition of the intermolecular potential.<sup>3</sup> The resulting MKNT expression for the steady state nucleation rate,  $J$ , is

$$J = A_{\text{kin}} \left[ \sum_{n=1}^{\infty} e^{-H(n)} \right]^{-1},$$

where the summation is over all cluster sizes  $n$  and  $A_{\text{kin}}$  is the standard prefactor in the Katz kinetic approach to nucleation<sup>35</sup>

$$A_{\text{kin}} = \rho_{\text{sat}}^v f_{\text{sat}} S,$$

$$f_{\text{sat}} = \frac{\rho_{\text{sat}}^v n_c^{2/3}}{\sqrt{2\pi m_1 k_B T}}.$$

Here  $n_c$  corresponds to the term bringing the major contribution to the sum (a critical cluster) and the function  $-H(n)$  describes the free energy of the  $n$ -cluster formation in  $k_B T$  units

$$-H(n) = \beta\Delta G(n) = -n \ln S + \theta_{\text{micro}} [\bar{n}^s(n) - 1]. \quad (6)$$

The pseudospinodal (solid line in Fig. 1) is given by<sup>32</sup>

$$\ln S_{\text{psp}}^{\text{MKNT}}(T) = \theta_{\text{micro}} \left( 1 - \frac{1}{q} \right), \quad q \equiv 1 + 2\omega + \omega\lambda. \quad (7)$$

The (temperature) range of validity of MKNT is given by the requirement

$$\left| \frac{B_2(T) p_{\text{sat}}(T)}{k_B T} \right| \ll 1, \quad (8)$$

implying according to Eq. (2) that  $e^{\theta_{\text{micro}}} \gg 1$ . For argon the criterion (8) gives  $T < 92$  K. Note that MKNT contains no adjustable parameters.

### C. Main features of the EMLD-DNT

EMLD-DNT of Reguera and Reiss<sup>22</sup> is a phenomenological approach where the critical cluster is diffusive rather than sharp as in the capillarity approximation of the CNT. The approach of a diffusive cluster is motivated by DFT calculations.<sup>36</sup>

The EMLD-DNT is based on a confined canonical system containing a sharp cluster and ideal vapor atoms. Such system represents the so-called EMLD cluster. The transition from the canonical system to the open, grand canonical system is achieved by allowing variations of the volume of the confinement sphere. In the DNT of Schenter *et al.*,<sup>15</sup> it is shown that the proper kinetic definition of the cluster volume is the one that minimizes its evaporation rate. In Ref. 22 it is demonstrated that such a choice for the cluster volume corresponds to the minimum of the change of the free energy with respect to the volume. Thus, in EMLD-DNT the free energy of the cluster is associated with the volume  $V_{\text{min}}$  of the confinement sphere which corresponds to the minimum of the local pressure.

The work of formation of this  $(N, V_{\text{min}})$  cluster at a temperature  $T$  is given by

$$\Delta G_{\text{EMLD-DNT}}^* = \Delta F - V_{\text{min}}(p - P_{\text{tot}}) + Nk_B T \ln(p/P_{\text{tot}}),$$

where  $\Delta F$  is the total Helmholtz free energy of the EMLD cluster,  $N$  is the total number of atoms in the confinement sphere, and  $P_{\text{tot}}$  is the total pressure of the EMLD cluster. Assuming that a sharp  $n$  cluster is described by the capillarity approximation, the work of its formation is

$$\Delta F(n) = -nk_B T \ln\left(\frac{p_1}{p_{\text{sat}}}\right) + \gamma_\infty s_1 n^{2/3} + nk_B T \left( 1 - \frac{p_{\text{sat}}}{\rho^l k_B T} \right) + Nk_B T \ln(p_1/p), \quad (9)$$

where  $p_1$  the ideal gas pressure of the remaining  $(N-n)$  vapor molecules in the sphere. The total free energy of the cluster is then calculated from the partition function of all possible sharp  $n$  clusters inside the confinement sphere

$$e^{-\beta\Delta F} = \sum_{n=0}^N e^{-\beta\Delta F(n)}.$$

The total pressure  $P_{\text{tot}}$  is the weighted sum over all  $n$  of the vapor phase pressure in the confinement sphere; the latter consists of  $p_1$  and the pressure exerted by the drop, modeled as a single ideal gas molecule moving within the container

$$P_{\text{tot}} = \sum_{n=0}^N f(n) \left[ p_1 + \frac{k_B T}{V_c} \Xi(n) \right].$$

Here  $V_c = 4\pi(R - r_n)^3/3$  is the volume accessible for the center of mass of the spherical  $n$  droplet with the radius  $r_n$ , and  $\Xi(n)$  is the unit step function. The weighting factor

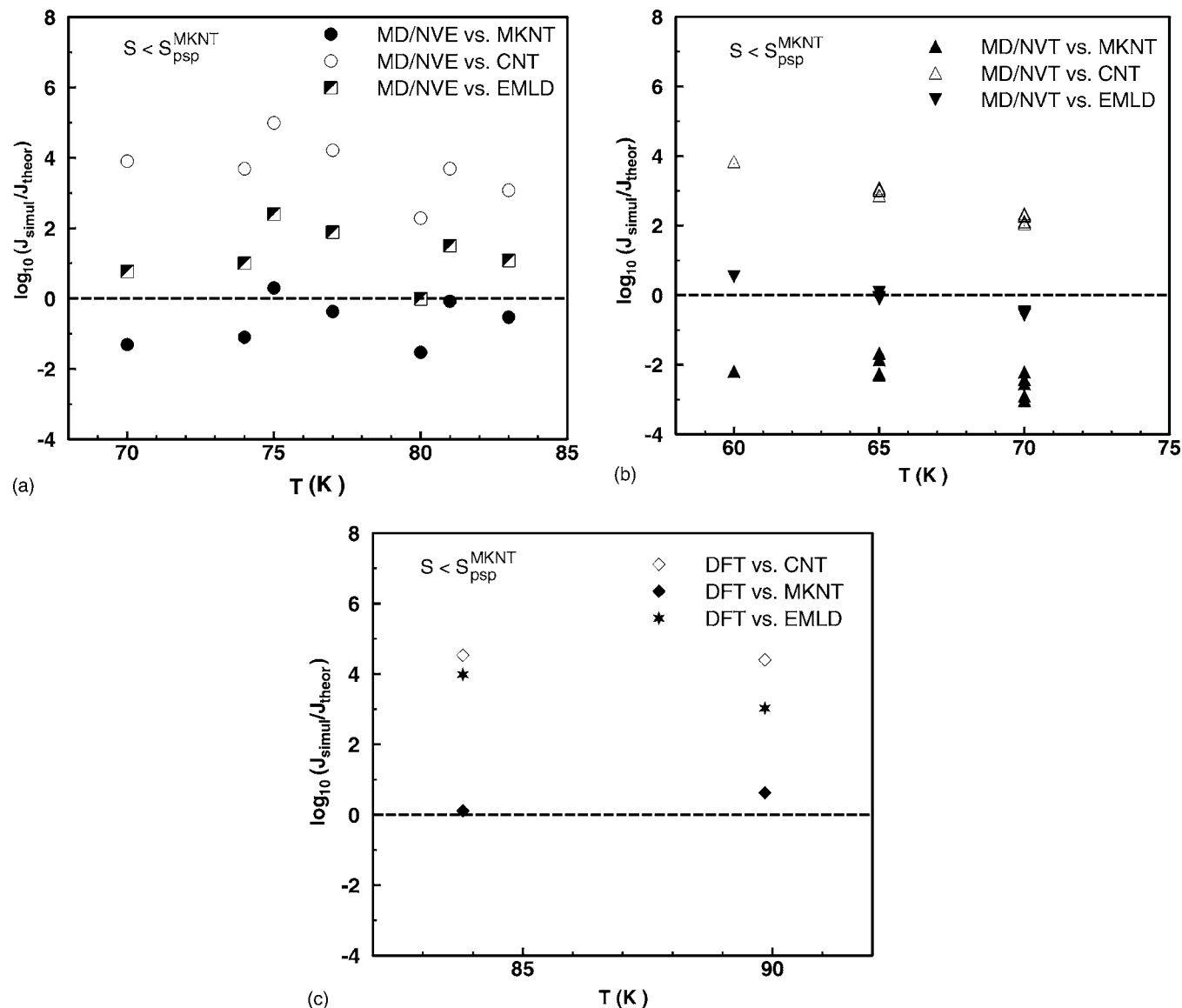


FIG. 2. MD simulations and DFT vs theory. (a) MD/NVE simulations of Ref. 24 vs theory, open circles: CNT, closed circles: MKNT, and semifilled squares: EMLD-DNT; (b) MD/NVT simulations of Ref. 25 vs theory, open triangles: CNT, filled upward triangles: MKNT, and filled downward triangles: EMLD-DNT; (c) DFT calculations of Ref. 13 vs theory, open rhombs: CNT, filled rhombs: MKNT, and filled stars: EMLD-DNT.

$$f(n) = \frac{e^{-\beta\Delta F(n)}}{\sum_{n=0}^N e^{-\beta\Delta F(n)}}$$

gives the probability of finding a drop of size  $n$ .  $P_{\text{tot}}$  is minimized to obtain  $V_{\text{min}}(N)$ . The nucleation rate reads

$$J_{\text{EMLD-DNT}} = K_{\text{CNT}} \exp\left(-\frac{\Delta G_{\text{EMLD-DNT}}^*}{k_B T}\right),$$

with the CNT kinetic prefactor,  $K_{\text{CNT}}$ .

## IV. RESULTS AND DISCUSSION

### A. Simulations and DFT versus theory

In accordance with the discussion in Sec. II, we present a comparison between theory and simulations for the domain of parameters

$$T < 92 \text{ K},$$

$$0 \leq \ln S \leq \ln S_{\text{psp}}^{\text{MKNT}}(T).$$

Figure 2 shows the relative nucleation rate  $\log_{10}(J_{\text{simul}}/J_{\text{theor}})$ , where  $J_{\text{simul}}$  is the nucleation rate found in MD/NVE simulations,<sup>24</sup> MD/NVT simulations,<sup>25</sup> and DFT calculations.<sup>13</sup> Open symbols correspond to the theoretical  $J$  given by the CNT and filled symbols refer to the nonclassical theoretical models. The dashed curve is the “ideal line”  $J_{\text{simul}}=J_{\text{theor}}$ . The agreement in the nucleation rate between MD simulations and the nonclassical models (MKNT and EMLD-DNT) in the whole temperature range is very good. For most of the simulations it is within 1–2 orders of magnitude, while the CNT rates are on average 3–5 orders of magnitude lower than the simulation results. At the same time MKNT demonstrates a perfect agreement (within one order of magnitude) with the DFT results while both the

classical theory and EMLD-DNT underestimate DFT data by 3–5 orders of magnitude. Note also that Fig. 2 shows that MKNT predicts a better temperature dependence of the nucleation rates compared to EMLD-DNT.

Comparison of the MD data at  $T=70$  K in Fig. 2 obtained in *NVE* (Ref. 24) and *NVT* (Ref. 25) simulations shows a difference of one order of magnitude. There are two possible reasons for this relatively small discrepancy. First, in the *NVT* simulations the nucleation rate is calculated from a mean first passage time analysis<sup>37</sup> (MFPT) while in the *NVE* simulations the threshold method is employed. It is known that these two methods yield up to one order of magnitude difference in the nucleation rate at given conditions.<sup>38</sup> Since the nucleation rate obtained by the threshold method is larger, it is located above the MFPT data in Fig. 1. Besides, in the *NVE* ensemble the latent heat heats up the system allowing for the natural temperature fluctuations, while in the *NVT* (or rather, isokinetic) simulations velocity scaling is applied, which forces the system to stay at a fixed temperature thereby not allowing temperature fluctuations.

It is important to determine the free energy barrier  $\Delta G^*$  from the cluster statistics obtained in simulations. Analysis of this quantity can provide information about the location of the nucleation point in the  $T$ – $S$  diagram with respect to the pseudospinodal (see Fig. 2). For low temperatures ( $T \leq 60$  K), the MD results presented in Table II of Ref. 24 (temperature, supersaturation, and the estimate of the corresponding critical cluster size  $n_c$ ) yield after the substitution into the MKNT free energy barrier [see Eq. (6)]:  $\beta\Delta G^* < 1$ . Consistently in Ref. 24, the critical cluster size for low  $T$  simulations is found to be close or even less than 1 molecule. The corresponding values of  $\Delta G^*$  for these conditions are expected to be  $\leq k_B T$  and, hence, the low-temperature simulations are in the spinodal nucleation domain.

Another important issue related to this discussion is an estimation of  $n_c$  from the nucleation rate  $J(T, S)$  using the nucleation theorem.<sup>39</sup> In order to do this one has to construct the isotherms  $J(S)_T$  and study the slopes of  $J$ – $S$  curves. Implementation of this procedure for the *NVE*-ensemble simulations is not straightforward since the temperature cannot be fixed, as opposed to the isokinetic ensemble. In general, it is always desirable to find a fit function for  $J(T, S)$  from the simulation data which then can be used to obtain the results for a wide range of parameters. However, in view of extremely high sensitivity of  $J$  to  $S$ , such a fit should preferably be an interpolation rather than an extrapolation to the domain where simulations were not performed as it has been discussed for simulations using different approaches for the fitting functions.<sup>24</sup>

## B. Experiment versus theory

In the first argon nucleation experiments in the cryogenic nucleation pulse chamber Fladerer and Strey<sup>8</sup> showed that the droplet growth at nucleation conditions for argon is too fast to decouple nucleation and growth by a pressure pulse. Therefore, no nucleation rate measurements were feasible. Nevertheless, Iland *et al.*<sup>9</sup> were able to estimate a nucleation rate range from the geometry of the detection system. Using

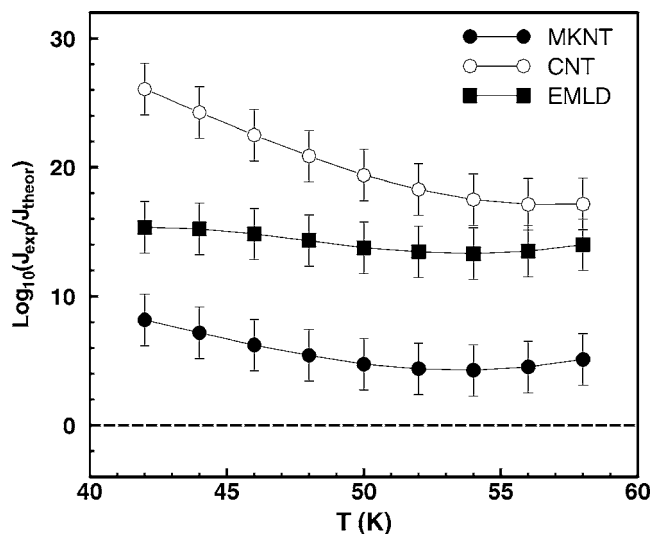


FIG. 3. Argon nucleation experiments of Iland *et al.* (Ref. 9) vs theory: CNT (open circles), EMLD-DNT (filled squares) (Ref. 25), and MKNT (filled circles).

the scattering volume of the order of  $10 \text{ nm}^3$  and the experience with the nucleation pulse chamber developed by Wagner and Strey<sup>40</sup> they defined a detectable droplet number density in the range of  $10^2 \leq N_d/\text{cm}^3 \leq 10^6$ . With a nucleation time of the order of  $\Delta t \approx 10^{-3} \text{ s}$  the experimental nucleation rate has to be  $10^5 \text{ cm}^{-3} \text{ s}^{-1} \leq J_{\text{exp}} = N_d/\Delta t \leq 10^9 \text{ cm}^{-3} \text{ s}^{-1}$ . All experimental measurements of Ref. 9 lie below the pseudospinodal line and thus can be analyzed using the CNT, MKNT, and EMLD-DNT. The relative (experiment versus theory) nucleation rates together with the error bars denoting the experimental accuracy are shown in Fig. 3. The agreement between all theoretical models and experiment is poor—4–8 orders of magnitude for MKNT, 12–14 orders for EMLD-DNT, and up to 26 orders for CNT.

## C. Overall comparison

This paper is aimed at obtaining a unified picture of argon nucleation combining different approaches. Unfortunately, in view of methodological reasons the experimental and simulation domains do not coincide and we have to carry out separate comparisons: Theory versus experiment and theory versus simulations and DFT. While the agreement of MKNT and EMLD-DNT with MD simulations is very good, the agreement between all theoretical models and experiment remains poor, though MKNT predictions are closer to experimental data than the other two models. The CNT deviates from simulations by approximately 3–5 orders of magnitude and from experiment by up to 26 orders.

As far as comparison with the DFT results is concerned, CNT and EMLD-DNT show approximately the same deviation of about 3–5 orders of magnitude while the MKNT agrees with the DFT perfectly. Recalling that the nucleation rate is very sensitive to the intermolecular interaction potential this agreement is quite remarkable since the DFT explicitly uses the (microscopic) interaction potential while the MKNT is a semiphenomenological model using as an input the macroscopic empirical EoS, the second virial coefficient,

the plain layer surface tension, and the coordination number in the bulk liquid. Note, however, that the amount of available DFT data is insufficient to formulate firm conclusions about the performance of different theoretical models.

It is highly desirable to bring together experiment and simulations—i.e., to perform simulations at lower  $S$  corresponding to the actual experimental conditions or to carry out nozzle experiments reaching higher supersaturations and nucleation rates. The main obstacle in simulations at low  $S$  is the necessity to simulate rare events requiring long computer times. Using the standard technique the vast majority of computational efforts is spent to simulate long waiting periods between rare nucleation events, so the accumulation of the appropriate statistics of such events becomes generally impossible. A solution to this problem could be an application of the “umbrella sampling” scheme<sup>41</sup> or the forward flux sampling (FFS) technique recently proposed by Allen *et al.*<sup>42</sup> The FFS methods allow computation of the rate constants and the transitions paths for equilibrium and nonequilibrium steady-state systems with stochastic dynamics. On the other hand, MC methods sample random configurations rather than the time dependent development of cluster formation in MD. The latter is more useful to investigate the dynamics of the nucleation and growth process as carried out in Refs. 24 and 25.

Since argon is a test system for assessment of various nucleation models, it is important to discuss general theories which are applicable to various substances, rather than substance-oriented models. The examples of such general models are CNT, MKNT, and EMLD-DNT discussed in the present paper; all of them contain no adjustable parameters. Several modifications of CNT are discussed in the literature. Apart from  $1/S$  Courtney’s correction<sup>43</sup> in the kinetic prefactor, which appears in the Katz kinetic approach to nucleation,<sup>35</sup> most of the modifications of the CNT deal with the various formulations of the free energy barrier  $\Delta G^*$ , which plays the dominant role in the nucleation behavior. One of the frequently discussed general modifications is the so-called “self-consistent CNT,” proposed by Girshick and Chiu<sup>44</sup> (GC) in which, similarly to the CNT, a cluster is approximated by a sharp single-step density profile, however, the barrier of the  $n$ -cluster formation is

$$\beta\Delta G_{GC}(n) = -n \ln S + \theta_\infty(n^{2/3} - 1). \quad (10)$$

It differs from the CNT expression (1) by the form of the surface contribution

$$\beta\Delta G_{GC}^{\text{surf}}(n) = \beta\Delta G_{CNT}^{\text{surf}}(n) - \beta\Delta G_{CNT}^{\text{surf}}(1), \quad (11)$$

where  $\beta\Delta G_{CNT}^{\text{surf}}(n) = \theta_\infty n^{2/3}$ . Equation (11) ensures that for a monomer  $\Delta G_{GC}^{\text{surf}}(n=1) = 0$ .

Indeed, to be consistent with the law of mass action a nucleation model should yield  $\Delta G^{\text{surf}}(n=1) = 0$  (see the detailed discussion in Ref. 45). However, the particular functional form, chosen in the GC model to satisfy this requirement, does not seem to be justified. Equations (10) and (11) are based on the assumption that the classical form of the barrier (1) is applicable to the cluster containing just one molecule,  $\beta\Delta G_{CNT}^{\text{surf}}(1) = \theta_\infty$ . Meanwhile, for small clusters the very concept of the plain layer (macroscopic) surface tension

loses its meaning and one has to apply microscopic (statistical mechanical) considerations instead of macroscopic (phenomenological) ones.

These considerations are used in MKNT. In the limit of small clusters the behavior of the barrier as a function of the cluster size  $n$  will be essentially different from the CNT form. As a result the surface part of the barrier for small clusters ( $n \leq N_1$ ) behaves not as  $\theta_\infty(T)(n^{2/3} - 1)$  (as in GC model) but as  $\theta_{\text{micro}}(T)(n - 1)$ . Thus, both the scaling law and the prefactor of the two models are different. Note, that the difference between  $\theta_\infty$  and  $\theta_{\text{micro}}$  can be substantial (e.g., for argon at  $T = 70$  K:  $\theta_\infty = 10.68$ ,  $\theta_{\text{micro}} = 4.96$ ). The size dependence of the cluster free energy is contained in the function  $\bar{n}^s(n)$  which is linear for small  $n$  and for  $n > N_1$  is a complicated (though analytical) function of  $n$  given by Eqs. (4) and (5); in the asymptotic limit of large clusters  $\bar{n}^s(n)$  scales as  $n^{2/3}$  corresponding to the compact spherical object. It is important to stress that in MKNT vanishing of  $\Delta G^{\text{surf}}$  at  $n = 1$  is not introduced as a correction into an earlier derived expression for  $\Delta G$  but results from statistical mechanical considerations. MKNT is an interpolative model which becomes exact in the limits of very small and very large clusters. Therefore, as any interpolative model, it is less accurate for clusters of intermediate sizes.

An obvious advantage of EMLD-DNT is that it uses the same set of phenomenological input parameters as the CNT:  $p_{\text{sat}}(T)$ ,  $\rho^l(T)$ ,  $\gamma_\infty(T)$ , but instead of a sharp density profile, EMLD-DNT allows for a diffusive cluster. This, however, results in a necessity to use the macroscopic classical form for the surface energy  $\gamma_\infty s_1 n^{2/3}$  for arbitrary clusters which becomes dubious for small  $n$ .

From experimental side one has to notice that the nucleation rates given in Ref. 9 are estimated and not obtained from the two signals—the transmitted and the scattered intensities—in combination with the Mie theory. The reason for this is shortly described in Sec. IV B as well as in Refs. 8 and 9. Since the expansion profile in the cryogenic chamber<sup>9</sup> is continuous it is probable that the measured signals describe the combined result of the newly born clusters and those grown from the earlier nucleation times. If this is the case, then it could explain (at least, partly) an overestimation of  $J$  compared to theoretical predictions. However, an overestimation of a few orders of magnitude will not be sufficient to considerably reduce the substantial discrepancy between the CNT and experiment.

## ACKNOWLEDGMENTS

We are indebted to a number of colleagues for illuminating discussions of the issues raised in this paper. It is a pleasure to thank H. Reiss, D. Kashchiev, and G. Wilemski for stimulating discussions of various aspects of nucleation theory. P. R. ten Wolde is acknowledged for sharing his knowledge of recent advances in computer simulation methods. We are grateful to J. Wedekind for providing the EMLD-DNT data for Figs. 2 and 3. A. Gleyzer and L. Goldenberg are acknowledged for carefully reading the manuscript and useful remarks. J.W. thanks R. Strey for his continuous support in all aspects of the work, both professional

and financial; his thoughts and suggestions are of great value. V.I.K. is grateful to J. Vrabec for useful communications concerning computational aspects of the paper and to D. Labetski for discussions of the data processing in nucleation experiments.

## APPENDIX: ARGON PROPERTIES

Molecular mass:  $M=39.948$  g/mol. Critical state parameters:<sup>1,9</sup>  $p_c=48.6$  bar,  $T_c=150.633$  K,  $\rho_c=13.29 \times 10^{-3}$  mol/cm<sup>3</sup>. Pitzer's acentric factor:<sup>1</sup>  $\omega_p=0.037$ . Equilibrium liquid mass density:<sup>9</sup>

$$\rho_{\text{mass}}^l = M(13.290 + 24.49248x^{0.35} + 8.155083x) \times 10^3 \text{ g/cm}^3,$$

$$x = 1 - \frac{T}{T_c}.$$

Saturation vapor pressure:<sup>9</sup>

$$\ln \frac{p_{\text{sat}}}{p_c} = \frac{T_c}{T} (-5.904188529x + 1.125495907x^{1.5} - 0.7632579126x^3 - 1.697334376x^6).$$

Surface tension:<sup>9</sup>

$$\gamma_\infty = 37.78x^{1.277} \text{ mN/m}.$$

LJ interaction parameters:<sup>46</sup>  $\sigma_{\text{LJ}}=3.405$  Å,  $\epsilon_{\text{LJ}}=119.8$  K. The second virial coefficient for nonpolar substances:<sup>1</sup>

$$\frac{B_2 p_c}{k_B T_c} = f_0 + \omega_p f_1,$$

$$f_0 = 0.1445 - 0.330/T_r - 0.1385/T_r^2 - 0.0121/T_r^3 - 0.000607/T_r^8,$$

$$f_1 = 0.0637 + 0.331/T_r^2 - 0.423/T_r^3 - 0.008/T_r^8,$$

where  $T_r=T/T_c$ .

<sup>1</sup>B. E. Poling, J. M. Prausnitz, and J. P. O'Connell, *The Properties of Gases and Liquids*, 5th ed. (McGraw-Hill, New York, 2001).

<sup>2</sup>J. S. Rowlinson and B. Widom, *Molecular Theory of Capillarity* (Clarendon, Oxford, 1982).

<sup>3</sup>V. I. Kalikmanov, *Statistical Physics of Fluids. Basic Concepts and Applications* (Springer, Berlin, 2001).

<sup>4</sup>D. Frenkel and B. Smit, *Understanding Molecular Simulation* (Academic, London, 1996).

<sup>5</sup>J. K. Johnson, J. A. Zollweg, and K. E. Gubbins, *Mol. Phys.* **78**, 591 (1993).

<sup>6</sup>R. Evans, *Adv. Phys.* **28**, 143 (1979).

<sup>7</sup>R. Evans, in *Fundamentals of Inhomogeneous Fluids*, edited by D. Henderson (Marcel Dekker, New York, 1992), p. 85.

<sup>8</sup>A. Fladerer and R. Strey, *J. Chem. Phys.* **124**, 164710 (2006).

<sup>9</sup>K. Iland, Ph.D. thesis, University of Köln, 2004; K. Iland, J. Wölk, R. Strey, and D. Kashchiev, *J. Chem. Phys.* **127**, 154506 (2007).

<sup>10</sup>R. Becker and W. Döring, *Ann. Phys.* **24**, 719 (1935); Ya. B. Zeldovich, *Acta Physicochim. URSS* **18**, 1 (1943).

<sup>11</sup>J. K. Lee, J. A. Baker, and F. F. Abraham, *J. Chem. Phys.* **58**, 3166 (1973).

<sup>12</sup>D. W. Oxtoby and R. Evans, *J. Chem. Phys.* **89**, 7521 (1988); D. W. Oxtoby, in *Fundamentals of Inhomogeneous Fluids*, edited by D. Henderson (Marcel Dekker, New York, 1992), Chap. 10.

<sup>13</sup>X. C. Zeng and D. W. Oxtoby, *J. Chem. Phys.* **94**, 4472 (1991).

<sup>14</sup>H. Reiss, A. Tabazadeh, and J. Talbot, *J. Chem. Phys.* **92**, 1266 (1990); C. L. Weakliem and H. Reiss, *ibid.* **99**, 5374 (1993).

<sup>15</sup>G. K. Schenter, S. M. Kathmann, and B. C. Garrett, *Phys. Rev. Lett.* **82**, 3484 (1999); *J. Chem. Phys.* **110**, 7951 (1999).

<sup>16</sup>S. M. Kathmann, G. K. Schenter, and B. C. Garrett, *J. Chem. Phys.* **116**, 5046 (2002).

<sup>17</sup>A. Dillmann and G. E. A. Meier, *J. Chem. Phys.* **94**, 3872 (1991).

<sup>18</sup>I. J. Ford, A. Laaksonen, and M. Kulmala, *J. Chem. Phys.* **99**, 764 (1993); C. F. Delale and G. E. A. Meier, *ibid.* **98**, 9850 (1993); V. I. Kalikmanov and M. E. H. van Dongen, *ibid.* **103**, 4250 (1995).

<sup>19</sup>M. E. Fisher, *Physics* (N.Y.) **3**, 255 (1967).

<sup>20</sup>K. Koga, X. C. Zeng, and A. K. Schekin, *J. Chem. Phys.* **109**, 4063 (1998).

<sup>21</sup>V. I. Kalikmanov, *J. Chem. Phys.* **124**, 124505 (2006).

<sup>22</sup>D. Reguera and H. Reiss, *Phys. Rev. Lett.* **93**, 165701 (2004).

<sup>23</sup>D. Reguera, R. K. Bowles, Y. Djikaev, and H. Reiss, *J. Chem. Phys.* **118**, 340 (2003).

<sup>24</sup>T. Kraska, *J. Chem. Phys.* **124**, 054507 (2006).

<sup>25</sup>J. Wedekind, J. Wölk, D. Reguera, and R. Strey, *J. Chem. Phys.* **127**, 154515 (2007).

<sup>26</sup>T. Kraska, *Ind. Eng. Chem. Res.* **43**, 6213 (2004).

<sup>27</sup>J. Kolafa and I. Nezbeda, *Fluid Phase Equilib.* **100**, 1 (1994).

<sup>28</sup>A. Linhart, C.-C. Chen, J. Vrabec, and H. Hasse, *J. Chem. Phys.* **122**, 144506 (2005).

<sup>29</sup>M. Mecke, J. Winkelmann, and J. Fischer, *J. Chem. Phys.* **107**, 9264 (1997).

<sup>30</sup>B. Smit, *J. Chem. Phys.* **96**, 8639 (1992).

<sup>31</sup>A. R. Imre, G. Meyer, G. Hazi, R. Rozas, and T. Kraska, *J. Chem. Phys.* (in press).

<sup>32</sup>V. I. Kalikmanov (unpublished).

<sup>33</sup>K. Binder, *Phys. Rev. A* **29**, 341 (1984).

<sup>34</sup>D. W. Oxtoby, *J. Phys.: Condens. Matter* **4**, 7627 (1992).

<sup>35</sup>J. L. Katz and H. Wiedersich, *J. Colloid Interface Sci.* **61**, 351 (1977).

<sup>36</sup>V. Talanquer and D. W. Oxtoby, *J. Chem. Phys.* **100**, 5190 (1994).

<sup>37</sup>J. Wedekind, R. Strey, and D. Reguera, *J. Chem. Phys.* **126**, 134103 (2007).

<sup>38</sup>R. Römer and T. Kraska, *J. Chem. Phys.* **127**, 234509 (2007).

<sup>39</sup>D. W. Oxtoby and D. Kashchiev, *J. Chem. Phys.* **100**, 7665 (1994).

<sup>40</sup>P. E. Wagner and R. Strey, *J. Chem. Phys.* **80**, 5266 (1984).

<sup>41</sup>P. R. ten Wolde and J. Frenkel, *Chem. Phys.* **109**, 9901 (1998).

<sup>42</sup>R. Allen, P. Warren, and P. R. ten Wolde, *Phys. Rev. Lett.* **94**, 018104 (2005); R. Allen, D. Frenkel, and P. R. ten Wolde, *J. Chem. Phys.* **124**, 194111 (2006).

<sup>43</sup>J. Courtney, *J. Chem. Phys.* **35**, 2249 (1961).

<sup>44</sup>S. Girshick and C.-P. Chiu, *J. Chem. Phys.* **93**, 1273 (1990).

<sup>45</sup>D. Kashchiev, *Nucleation. Basic Theory with Applications* (Butterworth, Oxford, 2000).

<sup>46</sup>A. Michels, H. Wijker, and H. Wijker, *Physica* **15**, 627 (1949).